Contrast Source Inversion of Non-Born Scatterers with Multi-Resolution Bayesian Learning

M. Salucci, L. Poli, F. Zardi, L.Tosi, S. Lusa, and A. Massa

2025/05/19

Contents

1 Comparison with IMSA-BCS vs. BARE-BCS

1.1 E-shaped Object, $\ell = 1.5\lambda$

Test Case Description

Direct solver:

- Side of the investigation domain: $L = 6.0\lambda$
- Cubic domain divided in $\sqrt{D} \times \sqrt{D}$ cells
- Number of cells for the direct solver: $D = 1600$ (discretization $= \lambda/10$)

Investigation domain:

- Cubic domain divided in $\sqrt{N} \times \sqrt{N}$ cells
- Number of cells for the inversion:

  - First Step IMSA: $N^{(1)} = 100$ (discretization $= \lambda/10$)

  - Following Steps IMSA: $N^{(i)}$ not fixed, defined according to the estimated *RoI* $\mathcal{D}^{(i)}$

Measurement domain:

- Total number of measurements: $M = 60$
- Measurement points placed on circles of radius $\rho = 4.5\lambda$

Sources:

- Plane waves
- Number of views: $V = 60$; $\theta_{inc}^{v} = 0 + (v-1) \times (360/V)$
- Amplitude: $A = 1.0$
- Frequency: $F = 300$ MHz ($\lambda = 1$)

Background:

- $\varepsilon_r = 1.0$
- $\sigma = 0$ [S/m]

Scatterer

- E-shaped object, $\ell = 1.5\lambda$
- $\varepsilon_r \in \{1.05,\ 1.10,\ 1.15, 1.20,\ 1.50,\ 2.00,\ 2.50\}$
- $\sigma = 0$ [S/m]

1.1.1 E-shaped Object, $\ell = 1.5\lambda$, $\tau = 0.10$ - IMSA-BCS vs. BARE-BCS reconstructed profiles

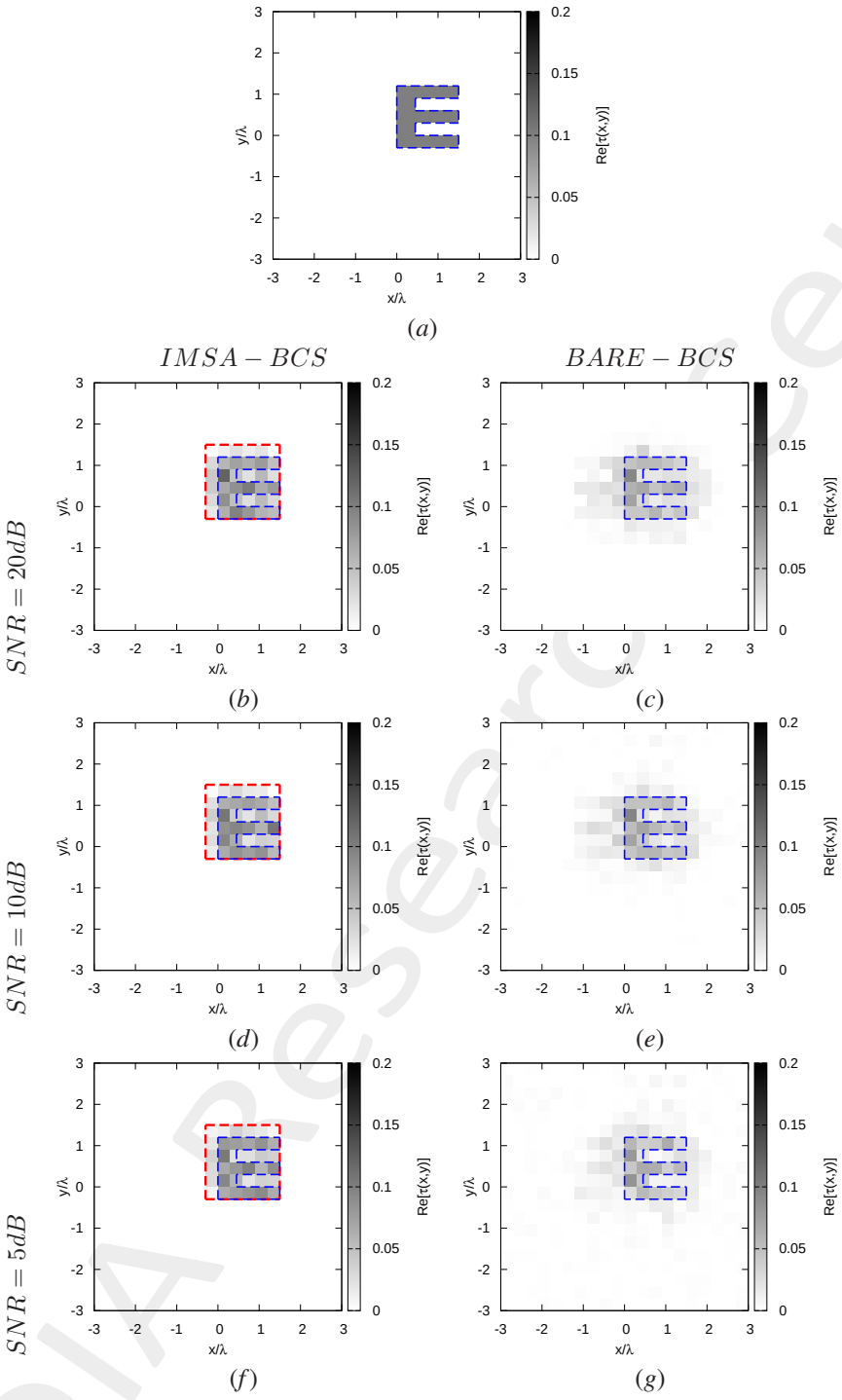

Figure 1: *E-shaped Object,* $\ell = 1.5\lambda$ *,*$\tau = 0.10$ - *IMSA-BCS vs. BARE-BCS* - (*a*) Actual profile, (*b*)(*d*)(*f*) $IMSA-BCS$ and $BARE-BCS$ reconstructed profiles for (*b*)(*c*) $SNR = 20$ [dB], (*d*)(*e*) $SNR = 10$ [dB] and (*f*)(*g*) $SNR = 5$ [dB].

	$SNR = 50dB$	
	$IMSA-BCS$	$BARE-BCS$
ξ_{tot}	2.38×10^{-3}	4.06×10^{-3}
ξ_{int}	2.57×10^{-2}	4.21×10^{-2}
ξ_{ext}	1.20×10^{-3}	2.15×10^{-3}
	$SNR = 20dB$	
	$IMSA-BCS$	$BARE-BCS$
ξ_{tot}	2.50×10^{-3}	4.11×10^{-3}
ξ_{int}	2.61×10^{-2}	4.28×10^{-2}
ξ_{ext}	1.31×10^{-3}	2.20×10^{-3}
	$SNR = 10dB$	
	$IMSA-BCS$	$BARE-BCS$
ξ_{tot}	2.27×10^{-3}	4.34×10^{-3}
ξ_{int}	2.30×10^{-2}	4.25×10^{-2}
ξ_{ext}	1.20×10^{-3}	2.32×10^{-3}
	$SNR = 5dB$	
	$IMSA-BCS$	$BARE-BCS$
ξ_{tot}	2.22×10^{-3}	5.08×10^{-3}
ξ_{int}	2.15×10^{-2}	4.61×10^{-2}
ξ_{ext}	1.21×10^{-3}	2.70×10^{-3}

Table I: *E-shaped Object,* $\ell = 1.5\lambda$*,* $\tau = 0.10$ - *IMSA-BCS vs. BARE-BCS* - Reconstrution errors: total (ξ_{tot}), internal (ξ_{int}) and external (ξ_{ext}) errors.

1.1.2 E-shaped Object, $\ell = 1.5\lambda$, $\tau = 0.20$ - IMSA-BCS vs. BARE-BCS reconstructed profiles

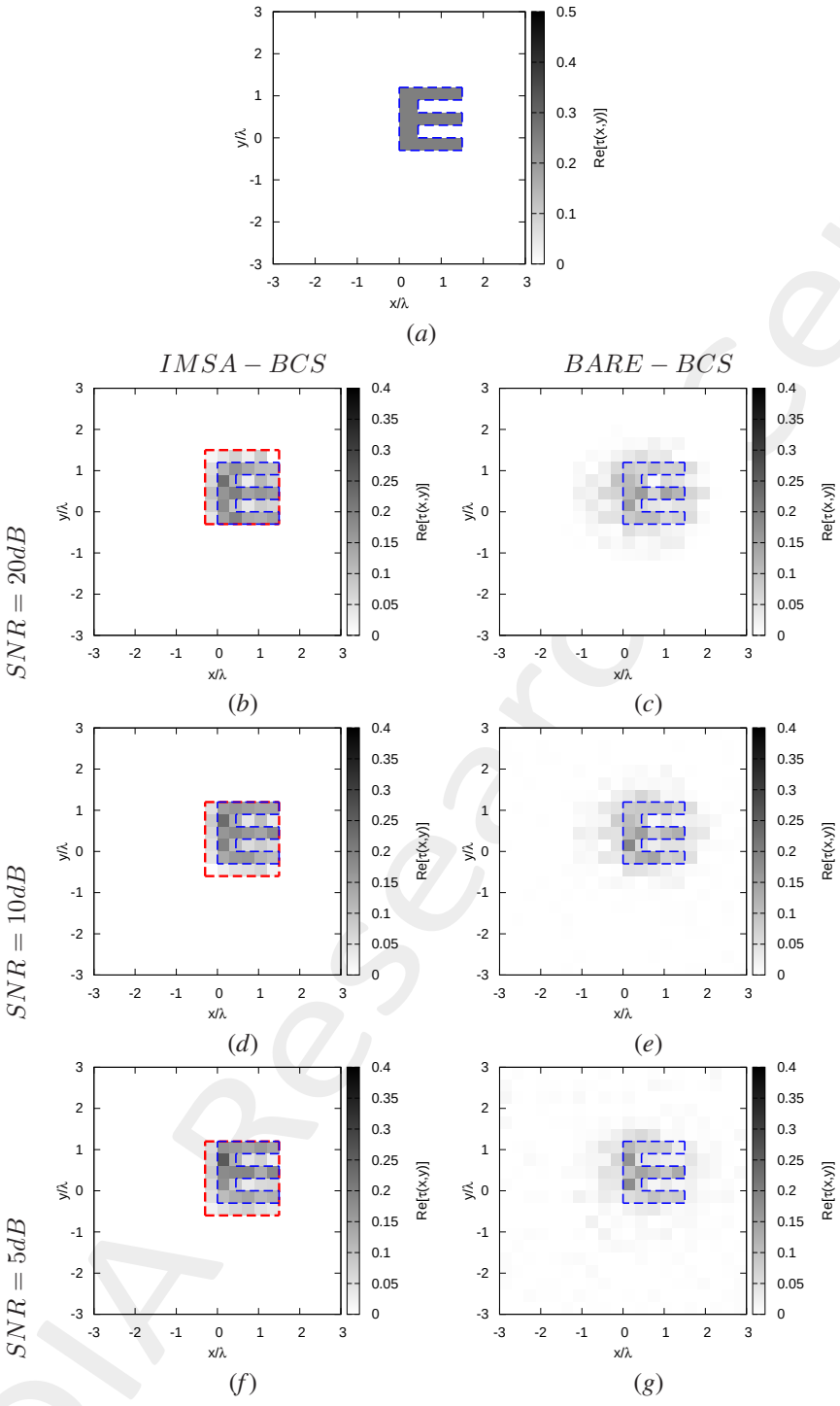

Figure 2: *E-shaped Object,* $\ell = 1.5\lambda$, $\tau = 0.20$ - *IMSA-BCS vs. BARE-BCS* - (*a*) Actual profile, (*b*)(*d*)(*f*) $IMSA-BCS$ and $BARE-BCS$ reconstructed profiles for (*b*)(*c*) $SNR = 20$ [dB], (*d*)(*e*) $SNR = 10$ [dB] and (*f*)(*g*) $SNR = 5$ [dB].

	$SNR = 50dB$	
	$IMSA-BCS$	$BARE-BCS$
ξ_{tot}	4.23×10^{-3}	8.89×10^{-3}
ξ_{int}	3.86×10^{-2}	8.55×10^{-2}
ξ_{ext}	2.40×10^{-3}	4.93×10^{-3}
	$SNR = 20dB$	
	$IMSA-BCS$	$BARE-BCS$
ξ_{tot}	4.82×10^{-3}	8.96×10^{-3}
ξ_{int}	4.38×10^{-2}	8.60×10^{-2}
ξ_{ext}	2.81×10^{-3}	5.01×10^{-3}
	$SNR = 10dB$	
	$IMSA-BCS$	$BARE-BCS$
ξ_{tot}	4.45×10^{-3}	9.26×10^{-3}
ξ_{int}	4.03×10^{-2}	7.96×10^{-2}
ξ_{ext}	2.55×10^{-3}	5.19×10^{-3}
	$SNR = 5dB$	
	$IMSA-BCS$	$BARE-BCS$
ξ_{tot}	4.62×10^{-3}	1.08×10^{-2}
ξ_{int}	4.36×10^{-2}	8.65×10^{-2}
ξ_{ext}	2.61×10^{-3}	5.92×10^{-3}

Table II: *E-shaped Object,* $\ell = 1.5\lambda$, $\tau = 0.20$ - *IMSA-BCS vs. BARE-BCS* - Reconstrution errors: total (ξ_{tot}), internal (ξ_{int}) and external (ξ_{ext}) errors.

1.1.3 E-shaped Object, $\ell = 1.5\lambda$, $\tau = 0.25$ - IMSA-BCS vs. BARE-BCS reconstructed profiles

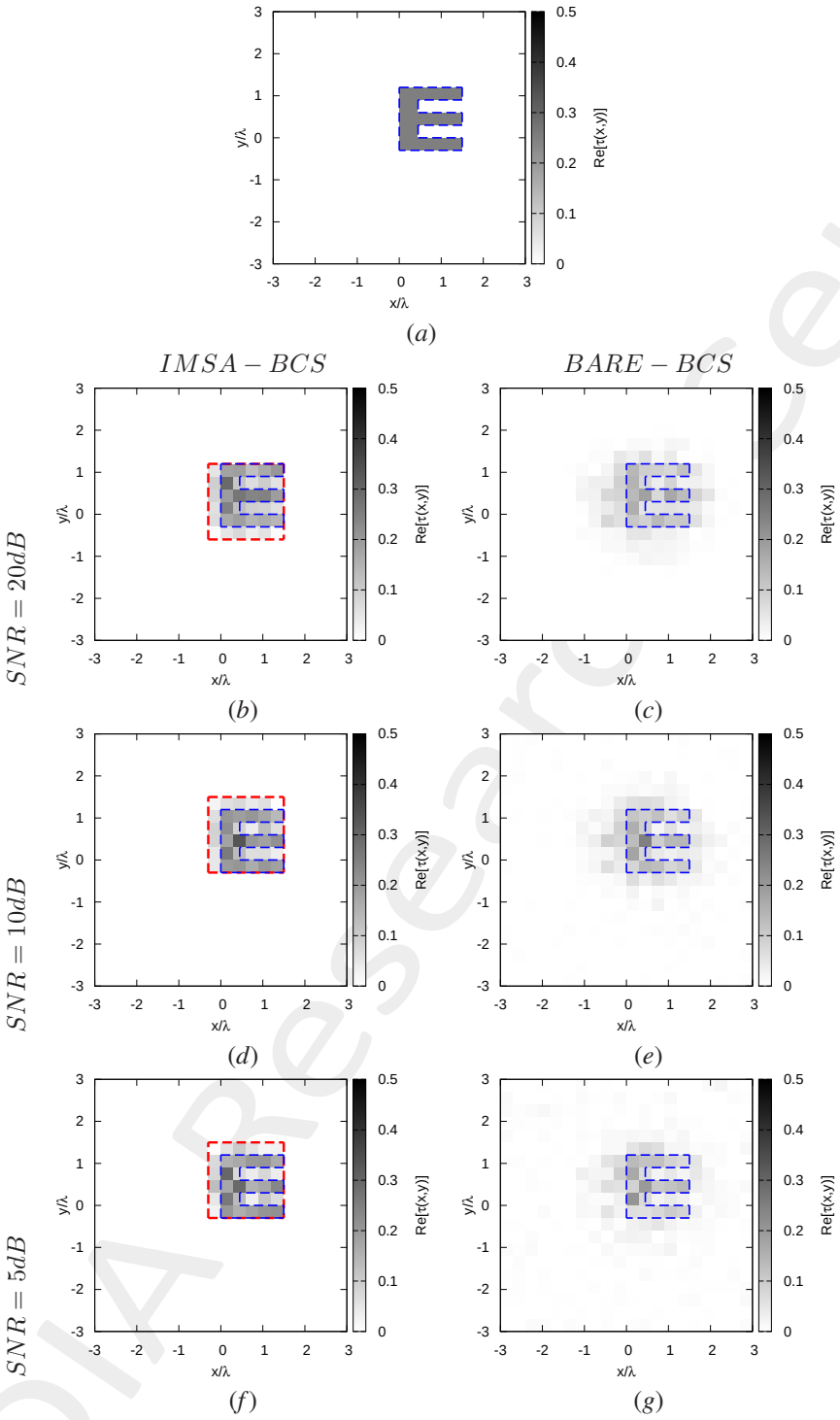

Figure 3: *E-shaped Object*, $\ell = 1.5\lambda$, $\tau = 0.25$ - *IMSA-BCS vs. BARE-BCS* - (*a*) Actual profile, (*b*)(*d*)(*f*) $IMSA-BCS$ and $BARE-BCS$ reconstructed profiles for (*b*)(*c*) $SNR = 20$ [dB], (*d*)(*e*) $SNR = 10$ [dB] and (*f*)(*g*) $SNR = 5$ [dB].

	$SNR = 50dB$	
	$IMSA-BCS$	$BARE-BCS$
ξ_{tot}	5.51×10^{-3}	1.13×10^{-2}
ξ_{int}	5.13×10^{-2}	1.09×10^{-1}
ξ_{ext}	3.04×10^{-3}	6.19×10^{-3}
	$SNR = 20dB$	
	$IMSA-BCS$	$BARE-BCS$
ξ_{tot}	5.50×10^{-3}	1.10×10^{-2}
ξ_{int}	5.15×10^{-2}	1.04×10^{-1}
ξ_{ext}	3.05×10^{-3}	6.22×10^{-3}
	$SNR = 10dB$	
	$IMSA-BCS$	$BARE-BCS$
ξ_{tot}	5.21×10^{-3}	1.22×10^{-2}
ξ_{int}	5.01×10^{-2}	1.02×10^{-1}
ξ_{ext}	2.88×10^{-3}	6.89×10^{-3}
	$SNR = 5dB$	
	$IMSA-BCS$	$BARE-BCS$
ξ_{tot}	5.61×10^{-3}	1.39×10^{-2}
ξ_{int}	5.17×10^{-2}	1.09×10^{-1}
ξ_{ext}	2.84×10^{-3}	7.61×10^{-3}

Table III: *E-shaped Object,* $\ell = 1.5\lambda$*,* $\tau = 0.25$ - *IMSA-BCS vs. BARE-BCS* - Reconstrution errors: total (ξ_{tot}), internal (ξ_{int}) and external (ξ_{ext}) errors.

1.2 Hollow Square, $\ell = 1.5\lambda$

Test Case Description

Direct solver:

- Side of the investigation domain: $L = 6.0\lambda$
- Cubic domain divided in $\sqrt{D} \times \sqrt{D}$ cells
- Number of cells for the direct solver: $D = 1600$ (discretization $= \lambda/10$)

Investigation domain:

- Cubic domain divided in $\sqrt{N} \times \sqrt{N}$ cells
- Number of cells for the inversion:

  - First Step IMSA: $N^{(1)} = 100$ (discretization $= \lambda/10$)

  - Following Steps IMSA: $N^{(i)}$ not fixed, defined according to the estimated *RoI* $\mathcal{D}^{(i)}$

Measurement domain:

- Total number of measurements: $M = 60$
- Measurement points placed on circles of radius $\rho = 4.5\lambda$

Sources:

- Plane waves
- Number of views: $V = 60$; $\theta_{inc}^{v} = 0 + (v-1) \times (360/V)$
- Amplitude: $A = 1.0$
- Frequency: $F = 300$ MHz ($\lambda = 1$)

Background:

- $\varepsilon_r = 1.0$
- $\sigma = 0$ [S/m]

Scatterer

- Hollow square object, $\ell = 1.5\lambda$
- $\varepsilon_r \in \{1.10,\ 1.20,\ 1.25\}$
- $\sigma = 0$ [S/m]

1.2.1 Hollow Square, $\ell = 1.5\lambda$, $\tau = 0.10$ - IMSA-BCS vs. BARE-BCS reconstructed profiles

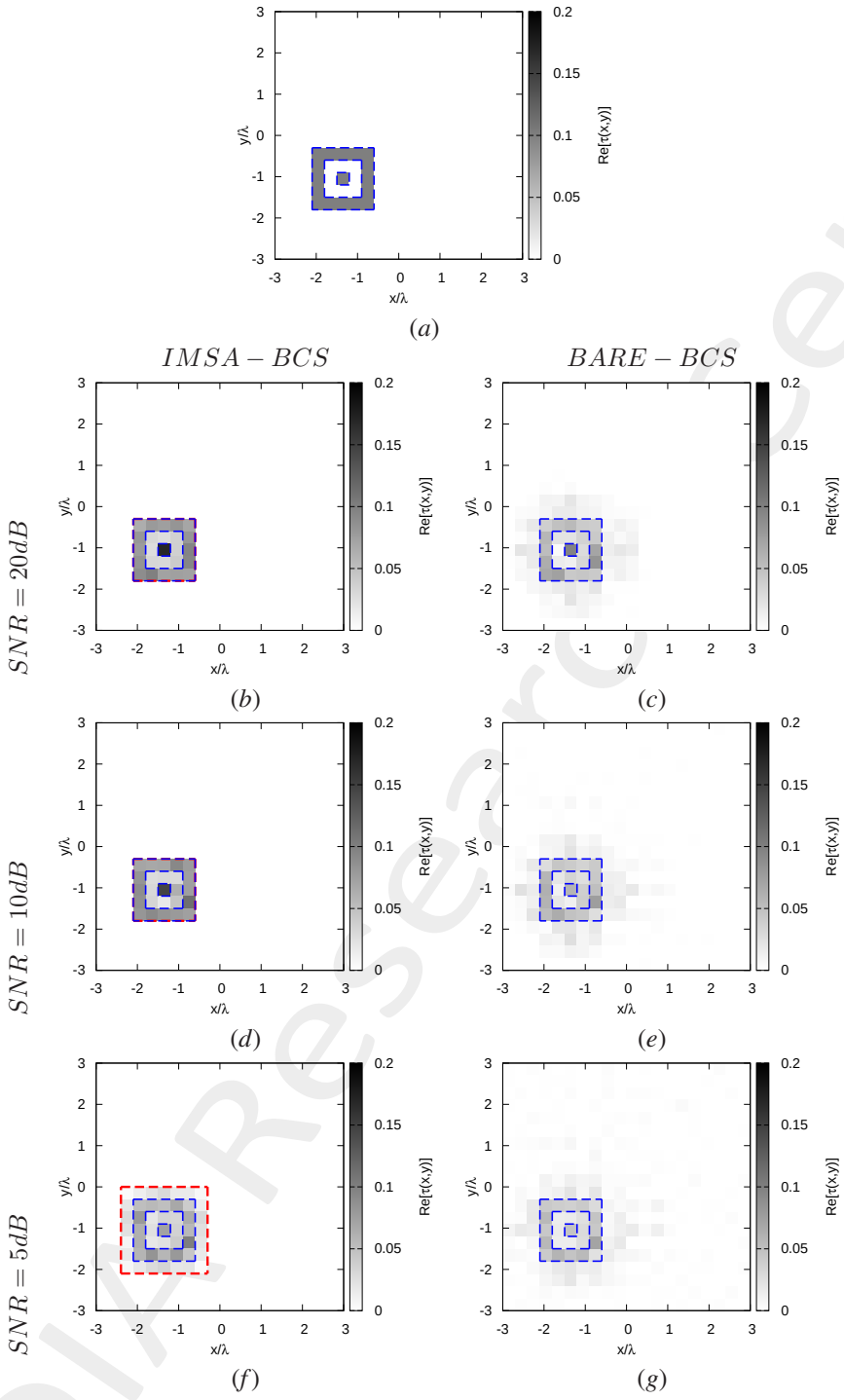

Figure 4: *Hollow Square*, $\ell = 1.5\lambda$, $\tau = 0.10$ - *IMSA-BCS vs. BARE-BCS* - (a) Actual profile, (b)(d)(f) $IMSA - BCS$ and $BARE - BCS$ reconstructed profiles for (b)(c) $SNR = 20$ [dB], (d)(e) $SNR = 10$ [dB] and (f)(g) $SNR = 5$ [dB].

	$SNR = 50dB$	
	$IMSA-BCS$	$BARE-BCS$
ξ_{tot}	1.58×10^{-3}	3.75×10^{-3}
ξ_{int}	2.17×10^{-2}	4.10×10^{-2}
ξ_{ext}	6.33×10^{-4}	2.00×10^{-3}
	$SNR = 20dB$	
	$IMSA-BCS$	$BARE-BCS$
ξ_{tot}	1.56×10^{-3}	3.63×10^{-3}
ξ_{int}	2.00×10^{-2}	3.96×10^{-2}
ξ_{ext}	6.82×10^{-4}	1.95×10^{-3}
	$SNR = 10dB$	
	$IMSA-BCS$	$BARE-BCS$
ξ_{tot}	1.56×10^{-3}	4.42×10^{-3}
ξ_{int}	1.94×10^{-2}	4.63×10^{-2}
ξ_{ext}	7.20×10^{-4}	2.38×10^{-3}
	$SNR = 5dB$	
	$IMSA-BCS$	$BARE-BCS$
ξ_{tot}	3.15×10^{-3}	5.03×10^{-3}
ξ_{int}	3.28×10^{-2}	4.93×10^{-2}
ξ_{ext}	1.75×10^{-3}	2.68×10^{-3}

Table IV: *Hollow Square*, $\ell = 1.5\lambda$, $\tau = 0.10$ - *IMSA-BCS vs. BARE-BCS* - Reconstrution errors: total (ξ_{tot}), internal (ξ_{int}) and external (ξ_{ext}) errors.

1.2.2 Hollow Square, $\ell = 1.5\lambda$, $\tau = 0.20$ - IMSA-BCS vs. BARE-BCS reconstructed profiles

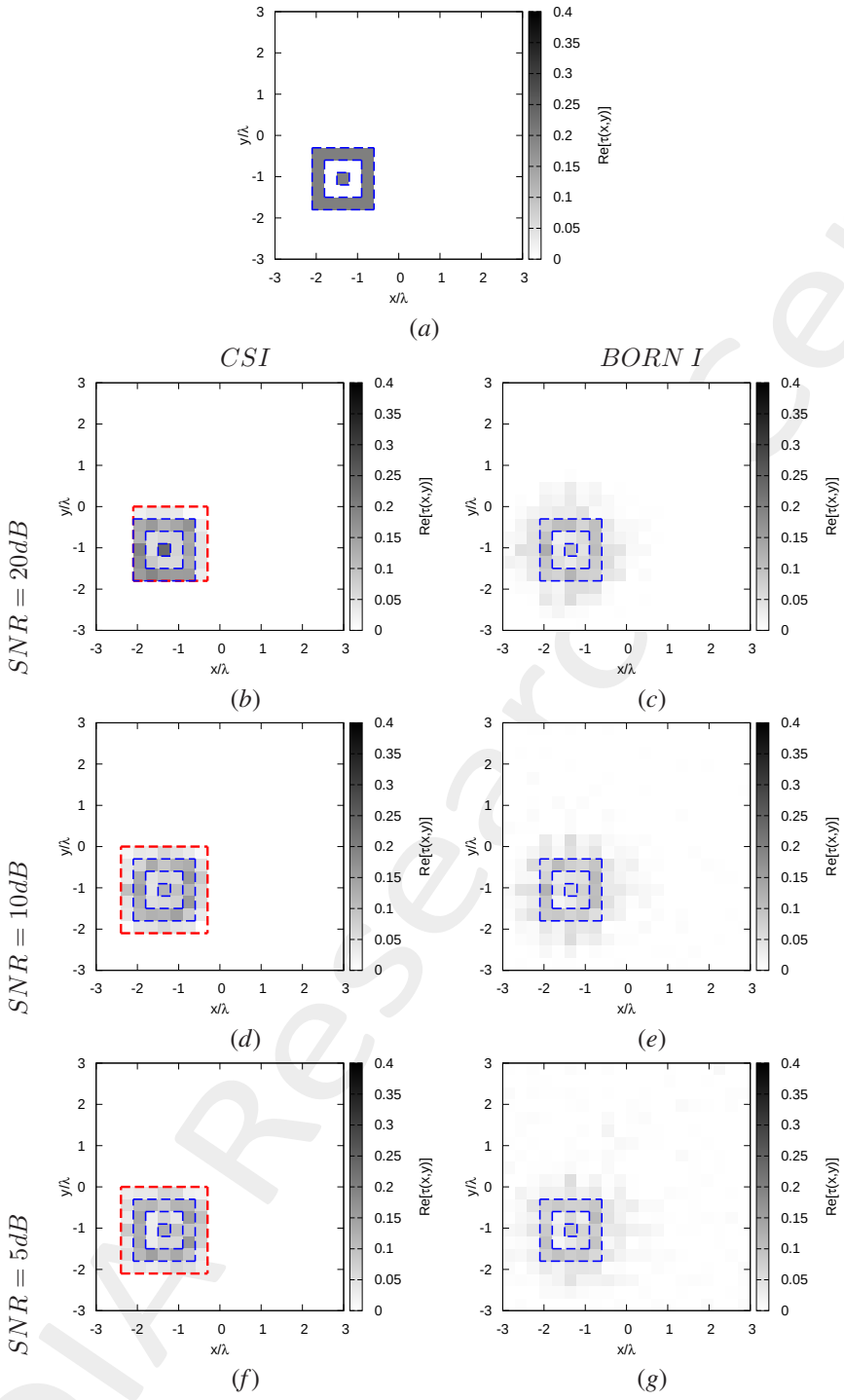

Figure 5: *Hollow Square*, $\ell = 1.5\lambda$, $\tau = 0.20$ - *IMSA-BCS vs. BARE-BCS* - (*a*) Actual profile, (*b*)(*d*)(*f*) $IMSA-BCS$ and $BARE-BCS$ reconstructed profiles for (*b*)(*c*) $SNR = 20$ [dB], (*d*)(*e*) $SNR = 10$ [dB] and (*f*)(*g*) $SNR = 5$ [dB].

	$SNR = 50dB$	
	$IMSA-BCS$	$BARE-BCS$
ξ_{tot}	4.48×10^{-3}	9.13×10^{-3}
ξ_{int}	4.44×10^{-2}	9.35×10^{-2}
ξ_{ext}	2.54×10^{-3}	5.12×10^{-3}
	$SNR = 20dB$	
	$IMSA-BCS$	$BARE-BCS$
ξ_{tot}	3.98×10^{-3}	8.99×10^{-3}
ξ_{int}	4.05×10^{-2}	9.06×10^{-2}
ξ_{ext}	2.23×10^{-3}	5.08×10^{-3}
	$SNR = 10dB$	
	$IMSA-BCS$	$BARE-BCS$
ξ_{tot}	6.72×10^{-3}	1.03×10^{-2}
ξ_{int}	6.62×10^{-2}	9.68×10^{-2}
ξ_{ext}	3.99×10^{-3}	5.82×10^{-3}
	$SNR = 5dB$	
	$IMSA-BCS$	$BARE-BCS$
ξ_{tot}	6.82×10^{-3}	1.14×10^{-2}
ξ_{int}	6.62×10^{-2}	9.76×10^{-2}
ξ_{ext}	4.02×10^{-3}	6.46×10^{-3}

Table V: *Hollow Square*, $\ell = 1.5\lambda$, $\tau = 0.20$ - *IMSA-BCS vs. BARE-BCS* - Reconstrution errors: total (ξ_{tot}), internal (ξ_{int}) and external (ξ_{ext}) errors.

1.2.3 Hollow Square, $\ell = 1.5\lambda$, $\tau = 0.25$ - IMSA-BCS vs. BARE-BCS reconstructed profiles

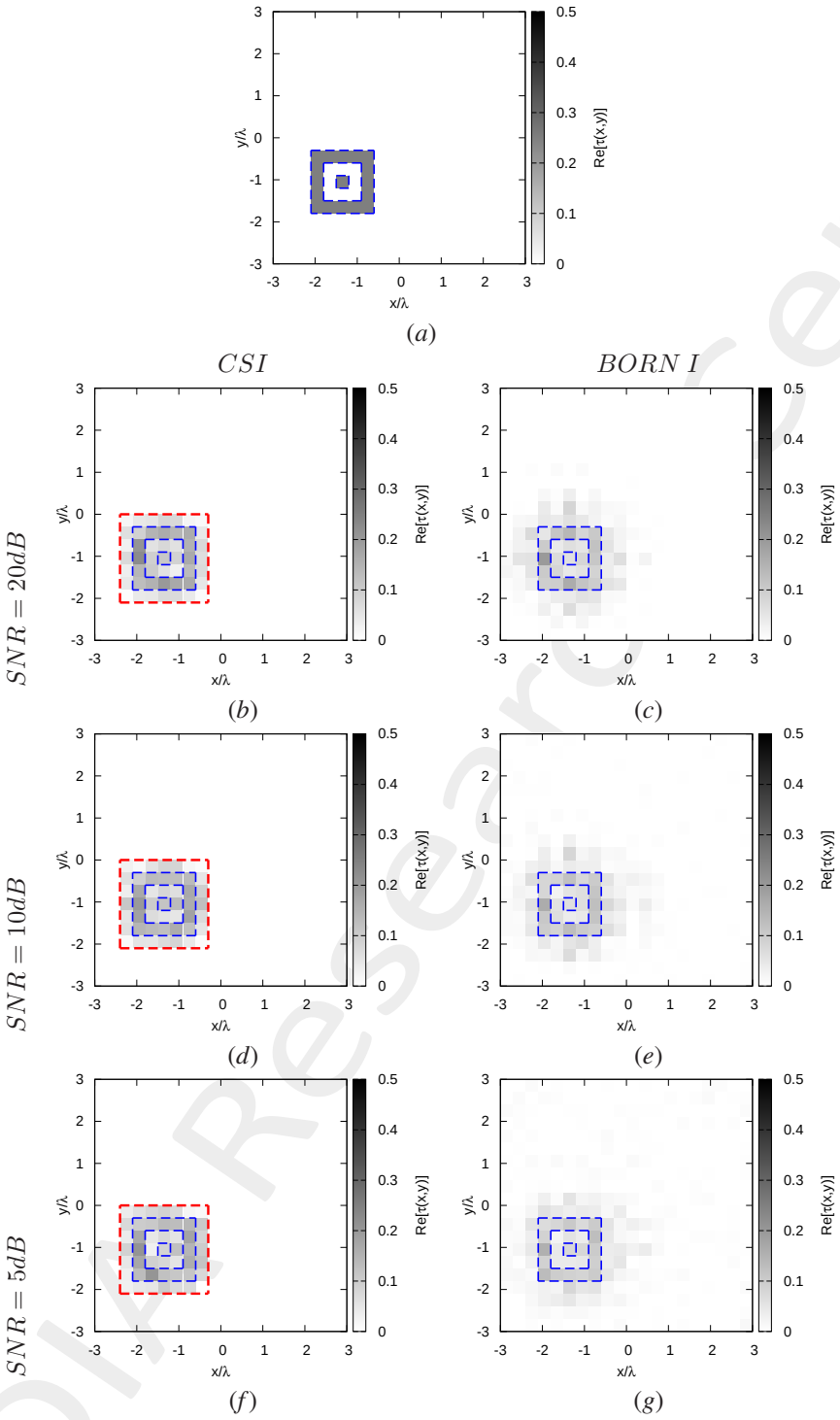

Figure 6: *Hollow Square*, $\ell = 1.5\lambda$, $\tau = 0.25$ - *IMSA-BCS vs. BARE-BCS* - (*a*) Actual profile, (*b*)(*d*)(*f*) $IMSA-BCS$ and $BARE-BCS$ reconstructed profiles for (*b*)(*c*) $SNR = 20$ [dB], (*d*)(*e*) $SNR = 10$ [dB] and (*f*)(*g*) $SNR = 5$ [dB].

	$SNR = 50dB$	
	$IMSA-BCS$	$BARE-BCS$
ξ_{tot}	7.40×10^{-3}	1.10×10^{-2}
ξ_{int}	7.43×10^{-2}	1.11×10^{-1}
ξ_{ext}	4.22×10^{-3}	6.19×10^{-3}
	$SNR = 20dB$	
	$IMSA-BCS$	$BARE-BCS$
ξ_{tot}	7.66×10^{-3}	1.14×10^{-2}
ξ_{int}	7.49×10^{-2}	1.13×10^{-1}
ξ_{ext}	4.45×10^{-3}	6.52×10^{-3}
	$SNR = 10dB$	
	$IMSA-BCS$	$BARE-BCS$
ξ_{tot}	8.52×10^{-3}	1.27×10^{-2}
ξ_{int}	8.31×10^{-2}	1.17×10^{-1}
ξ_{ext}	5.00×10^{-3}	7.25×10^{-3}
	$SNR = 5dB$	
	$IMSA-BCS$	$BARE-BCS$
ξ_{tot}	9.14×10^{-3}	1.45×10^{-2}
ξ_{int}	8.62×10^{-2}	1.21×10^{-1}
ξ_{ext}	5.42×10^{-3}	8.17×10^{-3}

Table VI: *Hollow Square*, $\ell = 1.5\lambda$, $\tau = 0.25$ - *IMSA-BCS vs. BARE-BCS* - Reconstrution errors: total (ξ_{tot}), internal (ξ_{int}) and external (ξ_{ext}) errors.

More information on the topics of this document can be found in the following list of references.

References

[1] G. Oliveri, M. Salucci, N. Anselmi, and A. Massa, "Compressive sensing as applied to inverse problems for imaging: theory, applications, current trends, and open challenges," *IEEE Antennas Propag. Mag. - Special Issue on 'Electromagnetic Inverse Problems for Sensing and Imaging,'* vol. 59, no. 5, pp. 34-46, Oct. 2017 (DOI: 10.1109/MAP.2017.2731204).

[2] A. Massa, P. Rocca, and G. Oliveri, "Compressive sensing in electromagnetics - A review," *IEEE Antennas Propag. Mag*., pp. 224-238, vol. 57, no. 1, Feb. 2015 (DOI: 10.1109/MAP.2015.2397092).

[3] A. Massa and F. Texeira, "Guest-Editorial: Special Cluster on Compressive Sensing as Applied to Electromagnetics," *IEEE Antennas Wirel. Propag. Lett.*, vol. 14, pp. 1022-1026, 2015 (DOI: 10.1109/LAWP.2015.2425011).

[4] M. Salucci, L. Poli, F. Zardi, L. Tosi, S. Lusa, and A. Massa, "Contrast source inversion of sparse targets through multi-resolution Bayesian compressive sensing," *Inverse Probl.*, vol. 40, no. 5, p. 055016, May 2024 (DOI 10.1088/1361-6420/ad3b33).

[5] G. Oliveri, N. Anselmi, M. Salucci, L. Poli, and A. Massa, "Compressive sampling-based scattering data acquisition in microwave imaging," *J. Electromagn. Waves Appl.* J, vol. 37, no. 5, 693-729, Mar. 2023 (DOI: 10.1080/09205071.2023.2188263).

[6] G. Oliveri, L. Poli, N. Anselmi, M. Salucci, and A. Massa, "Compressive sensing-based Born iterative method for tomographic imaging," *IEEE Tran. Microw. Theory Techn.*, vol. 67, no. 5, pp. 1753-1765, May 2019 (DOI: 10.1109/TMTT.2019.2899848).

[7] M. Salucci, L. Poli, and G. Oliveri, "Full-vectorial 3D microwave imaging of sparse scatterers through a multi-task Bayesian compressive sensing approach," *Journal of Imaging*, vol. 5, no. 1, pp. 1-24, Jan. 2019 (DOI: 10.3390/jimaging5010019).

[8] M. Salucci, A. Gelmini, L. Poli, G. Oliveri, and A. Massa, "Progressive compressive sensing for exploiting frequency-diversity in GPR imaging," *J. Electromagn. Waves Appl. J*, vol. 32, no. 9, pp. 1164-1193, 2018 (DOI: 10.1080/09205071.2018.1425160).

[9] N. Anselmi, L. Poli, G. Oliveri, and A. Massa, "Iterative multi-resolution bayesian CS for microwave imaging," *IEEE Trans. Antennas Propag.*, vol. 66, no. 7, pp. 3665-3677, Jul. 2018 (DOI: 10.1109/TAP.2018.2826574).

[10] N. Anselmi, G. Oliveri, M. A. Hannan, M. Salucci, and A. Massa, "Color compressive sensing imaging of arbitrary-shaped scatterers," *IEEE Trans. Microw. Theory Techn.*, vol. 65, no. 6, pp. 1986-1999, Jun. 2017 (DOI: 10.1109/TMTT.2016.2645570).

[11] N. Anselmi, G. Oliveri, M. Salucci, and A. Massa, "Wavelet-based compressive imaging of sparse targets," *IEEE Trans. Antennas Propag.*, vol. 63, no. 11, pp. 4889-4900, Nov. 2015 (DOI: 10.1109/TAP.2015.2444423).

[12] G. Oliveri, P.-P. Ding, and L. Poli, "3D crack detection in anisotropic layered media through a sparseness-regularized solver," *IEEE Antennas Wirel. Propag. Lett.*, vol. 14, pp. 1031-1034, 2015 (DOI: 10.1109/LAWP.2014.2365523).

[13] L. Poli, G. Oliveri, P.-P. Ding, T. Moriyama, and A. Massa, "Multifrequency Bayesian compressive sensing methods for microwave imaging," *J. Opt. Soc. Am. A*, vol. 31, no. 11, pp. 2415-2428, 2014 (DOI: 10.1364/JOSAA.31.002415).

[14] G. Oliveri, N. Anselmi, and A. Massa, "Compressive sensing imaging of non-sparse 2D scatterers by a total-variation approach within the Born approximation," *IEEE Trans. Antennas Propag.*, vol. 62, no. 10, pp. 5157-5170, Oct. 2014 (DOI: 10.1109/TAP.2014.2344673).